This is a repository copy of *Nonlinear dynamic response and modeling of a bi-stable composite plate for applications to adaptive structures*.

Nonlinear dynamic response and modelling of a bi-stable composite plate for applications to adaptive structures

A. F. Arrieta · S. A. Neild · D. J. Wagg

Abstract This paper discusses the formulation and validation of a low order model to capture the dynamics of a bi-stable composite plate, focusing on the dynamics around its stable states. More specifically, the model aims to capture the complex nonlinear subharmonic behaviour observed in the dynamic response of the plate. A system identification approach is used to derive simplified equations of motion for the system. Experimental frequency response diagrams are obtained to characterize the observed dynamics in the identification process. Simulations using the identified model are presented showing excellent agreement with the experimentally observed behaviour. A theoretical validation of the model is carried out studying the stability of the modes where subharmonic response was observed. Stability boundaries were computed using averaging techniques showing good agreement with experimental results.

1 Introduction

The ever growing need for better performing systems has resulted in the integration of various disciplines such as dynamics, control and material science to accomplish superior solutions for engineering problems. This integrated design philosophy has resulted in the research field of adaptive structures [4]. Composite materials have played an important roll in the progress of adaptive structure technologies. In aerospace engineering, structures made from composite laminates are increasingly important in a wide variety of applications, including morphing adaptive structures.

One promising advance is the development of curved composite laminate plates which have multiple stable shapes resulting from asymmetric residual thermal stresses

A. F. Arrieta
Department of Mechanical Engineering, University of Bristol, University Walk, Bristol, U.K. BS8 1TR
Tel.: +44(0)1173317601
E-mail: andres.arrietadiaz@bristol.ac.uk

induced during the curing process [5]. The property of multi-stability has led to these materials being considered for use in a range of adaptive structures, particularly for morphing aerospace structures [24]. Recent research suggests that by designing the induced thermal stresses the production of a wide range of desired stable shapes is becoming feasible [23] and aerospace applications using this design morphing capabilities have been introduced [16]. The change between stable states for the bi-stable plate is achieved by a snap-through mechanism which is strongly nonlinear in nature [26]. Most of the studies of bi-stable composite laminates for morphing applications have focused on modelling the shape after the manufacturing process and their static characteristics [6,12]. More specifically, these studies have focused on the identification of the stiffness characteristics [10,17] and snap-through loading [7,22]. However, the operating conditions for aerospace morphing applications will inevitably lead the plate structures to be exposed to high levels of dynamic excitation in an aeroelastic environment. In particular, undesired vibration could induce early failure of the structures generating the need for vibration suppression mechanisms, for example the control system presented in [21].

The successful implementation of such control strategies relies on accurate models describing the dynamics of the structures. However, vibration suppression control has not been attempted on multi-stable composite laminates to the knowledge of the authors. Furthermore, very little (if any) work has been carried out to examine the dynamics of bi-stable composite plates and no dynamic models have been presented. The object of this paper is to derive a simple low order model to capture the key dynamic features of a of bi-stable composite laminate plate. In particular, we focus on the study of the dynamic properties around the stable-states of a square bi-stable carbon-fiber epoxy $[0_O^4 - 90_O^4]_T$ plate. In the future, this model will be used along with adaptive control strategies to implement composite laminate based morphing applications. This study complements the paper on snap-through dynamics presented by [1].

A novel system identification approach based on experimental frequency response diagrams is employed to capture the main dynamic characteristics of the bi-stable plate, such as primary resonance and damping coefficients. Based on previous studies on shallow shells [20] the identification process was extended to include secondary subharmonic resonance observed in nonlinear vibration of flexible flat composite plates and curved beams [8]. Moreover, large responses due to subharmonic vibrations can lead to catastrophic failure of aerospace structures even if the excitation is away from the natural frequencies of the system as reported in [14,29], and therefore must be included in a complete dynamic model.

The result of the experimental identification process is a set of nonlinear coupled second-order differential-equations capable of describing the main dynamic features for the bi-stable composite plate. Simulations based on the identified set of equations along with a study of the subharmonic resonance are presented to validate the model.

In Section 2 the experimentally measured frequency response diagrams are presented and the system identification process used to obtain the equations of motion for the bi-stable plate is described. Section 3 presents simulated frequency response diagrams and compares them to the experimental results. In Section 4 a subharmonic resonance stability boundary analysis for the identified model is conducted and compared to the measured values. Finally, in section 5 conclusion are drawn and future work discussed.

2 Low Order Modeling: a system identification approach

A low order model which captures the key dynamic behaviour of a bi-stable composite plate is determined based on an experimental system identification approach for low order systems [13,15]. The two stable states of the bi-stable plate are shown in figure 1. This identification process consisted in obtaining experimental frequency response diagrams for the dynamic response to sinusoidal excitations in order to characterize the behaviour a number of points in the plate. This process was performed for both stable states, which exhibited almost symmetrical response characteristics. Therefore, the whole process will be developed using the set of experiments obtained for one of the stable states. The main aim of the model is to capture the out of plane displacement for the low frequency response of the plate.


(a) Stable state 1   (b) Stable state 2
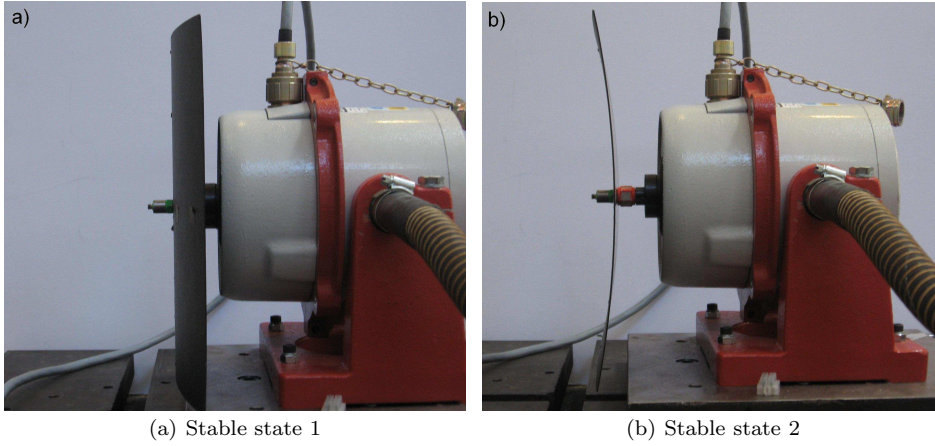
Fig. 1 Stable states of the Bi-stable plate.

2.1 Experimental Assembly and Measurement Procedure

Assembly A carbon-fibre epoxy $[0_4-90_4]_T$ 300x300 [mm] square bi-stable laminate was used as the experimental specimen. The laminate tested was attached to a Ling shaker in order to induce vibration to the system. A differential laser vibrometer measured the relative displacement between the centre and a given point on the laminate. The experimental arrangement was mounted on a steel table of large mass in order to ensure no interaction between the plate and its surroundings as seen in figure 2.

Measurement Procedure The plate was characterized by measuring experimental frequency response for 2 points on the coordinate directions of a local frame as shown schematically in figure 3. Point P_x characterizes the response of the curved direction, which coincides with x coordinate in the chosen reference frame. The point P_y captures the response of the flat direction of the plate, coinciding with the y coordinate in the reference frame. Measurements are made relative to the origin, point o, in the plate.
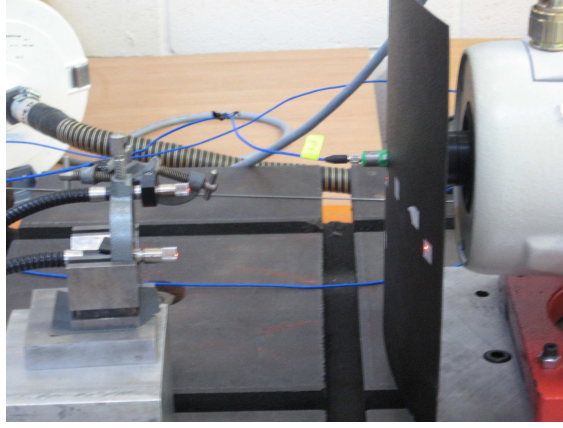
Fig. 2 Experimental Assembly. Ling shaker V405, vibrometer OFV-552
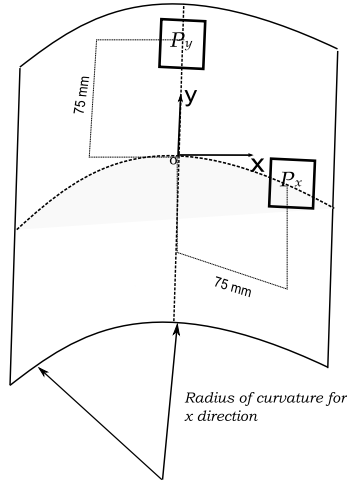
Fig. 3 Measured points in the laminate. Point P_x describes the out-of-plane vibration in curved direction , coinciding with the x-coordinate. Point P_y describes the out-of-plane vibration in the flat direction, coinciding with the y-coordinate.

The frequency response diagrams for the system were carried out using a stroboscopic sampling of the time series for the measured displacement data. By exciting the system with a sinusoidal signal to induce vibration, peak-to-peak displacement measurements were sampled from the time responses for several forcing periods, as shown in figure 4(a). The stroboscopic sampling frequencies during the experiment were set to the forcing frequency. For every sampling frequency the stroboscopic sampling process was repeated over ten consecutive steady-state forcing periods. A single point in a frequency response diagram represents the sampled amplitude value over one forcing period. For a linear system the sampled amplitude for a given forcing frequency over consecutive forcing periods remains the same. In contrast, a nonlinear system can have a response with multiple measured amplitudes for a given forcing frequency over consecutive forcing periods as seen in figure 4(b).
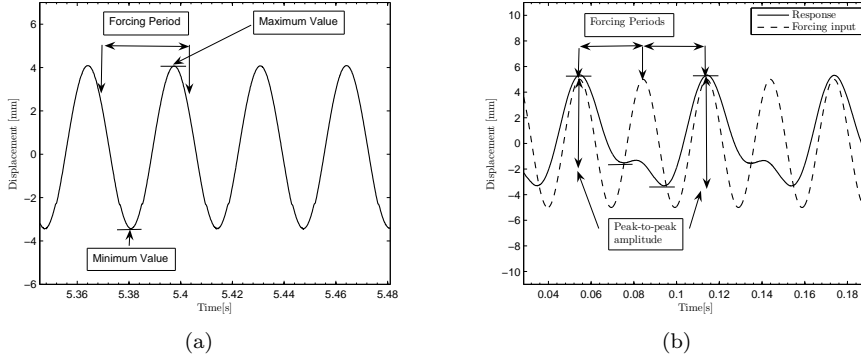
Fig. 4 Stroboscopic sampling procedure to obtain peak-to-peak values for a given forcing period. For a) a linear response and b) a nonlinear response.

2.2 System Identification

The system identification process focused on identifying the dominant modes of the plate, their damping coefficients and the existence of important nonlinear oscillations in the response. Initially, we obtained a low amplitude experimental frequency response function (FRF) for the frequency range of interest to identify the relevant modes for both direction of the plate assuming a linear behaviour following standard modal testing procedures [9]. The FRF obtained for the curved direction is presented in figure 5. Two dominant modes of vibration can be seen, mode X_1 at 17.6 Hz and mode X_2 at 45.4 Hz. Damping coefficients ζ_{x_1} and ζ_{x_2}, are chosen based on the peaks for the response for each mode.

In order to identify nonlinear oscillations in the parameter range of study experimental frequency response diagrams were obtained for a range of forcing amplitudes and frequencies of [0.5,5] N and [13,43] Hz respectively. A linear feedback proportional controller was implemented to ensure the desired forcing amplitude over the required range of frequencies. This eliminates any dynamic coupling effects which could be introduced by the Ling Shaker.

The frequency response diagram for point P_x describing the response of the curved (x) direction of the plate for an input force amplitude of 5 N is shown in figure 6. The response resembles the results obtained for the linear FRF except for the region around 35 Hz. This range coincides with twice the natural frequency for mode X_1. In more detail the nonlinear displacement response for point P_x at 34.2 Hz shown in figure 7(a). A non sinusoidal response to the harmonic excitation of the plate is observed. The measured power spectrum of the response, presented in figure 7(b), shows that most of the energy transmitted by the external forcing at 34.2 Hz is transferred to a lower frequency at around 17.6 Hz. This coincides with the measured frequency of mode X_1. The features observed during the identification process suggest that the nonlinear behaviour is due to a 1/2 subharmonic response of mode X_1 [18].

The frequency response diagram for point P_y describing the flat (y) direction of the plate can be seen in figure 8. In this case the dynamics are dominated by a single mode, mode Y_1 at 19.6 Hz. As with mode X_1, ζ_{y_1} is chosen based on the peak for the response of mode Y_1. As for the curved direction of the plate, a nonlinear response is found
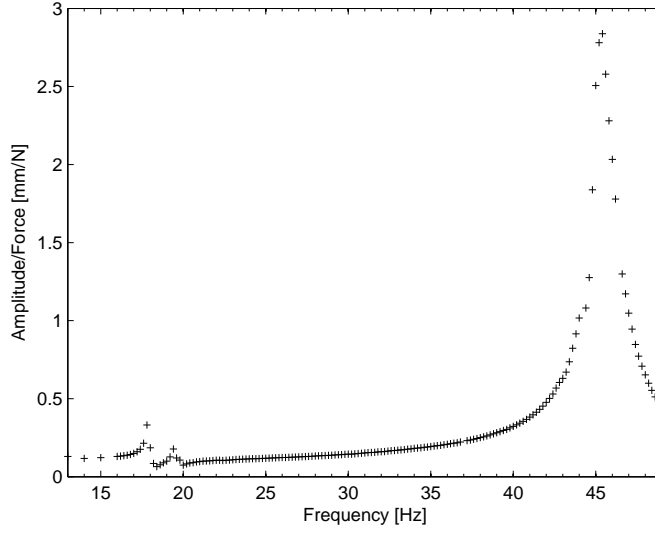
Fig. 5 Experimental receptance (Displacement/Force) FRF for the curved (x) direction, point P_x. Forcing amplitude $F_o = 1.0$ N, frequency range $\Omega=[13, 49]$
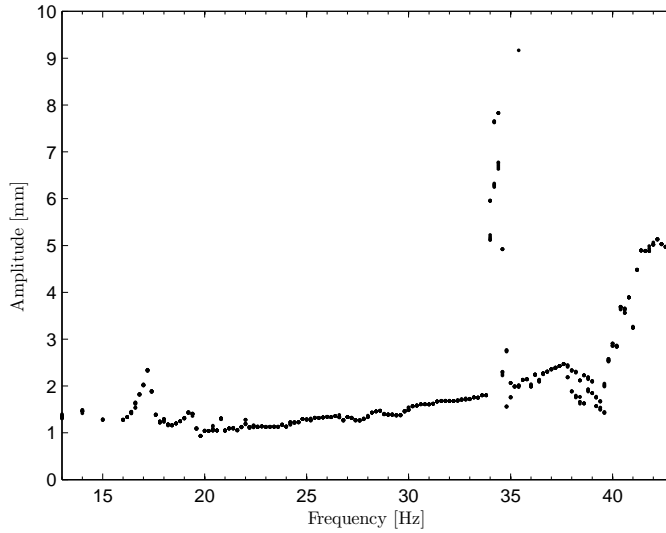
Fig. 6 Experimental frequency response for the curved (x) direction, point P_x. F_o=5.0 N, frequency range $\Omega=[13, 43]$

around the range of twice the frequency of mode Y_1. An example displacement time series, figure 9(a), displays a harmonic response, however the power spectrum graph (figure 9(b)) shows, once again, that most of the energy from the forcing is transferred from the higher forcing frequency (at 39.2 in this case) to the lower frequency at
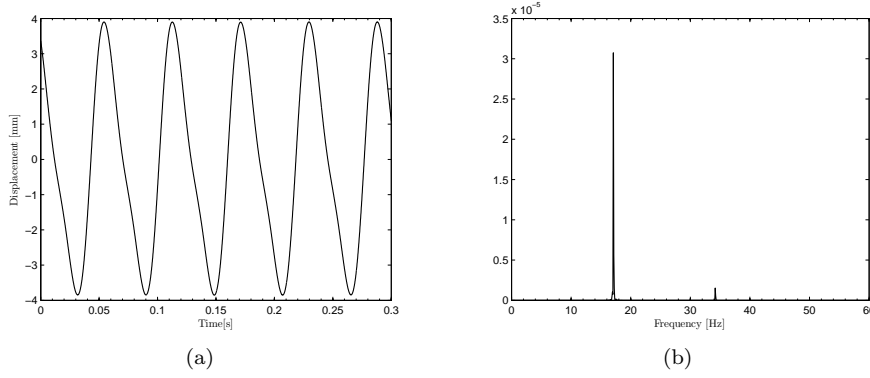
Fig. 7 Experimentally recorded dynamic response for the curved (x) direction, point P_x. Forcing amplitude F_o=5 N, forcing frequency Ω=34.2 Hz. (a) displacement time response. (b) displacement power spectrum.

around 19 Hz, coinciding with the frequency of mode Y_1. Once more, the experimentally observed characteristics agree with that of a 1/2 subharmonic behaviour of mode Y_1.
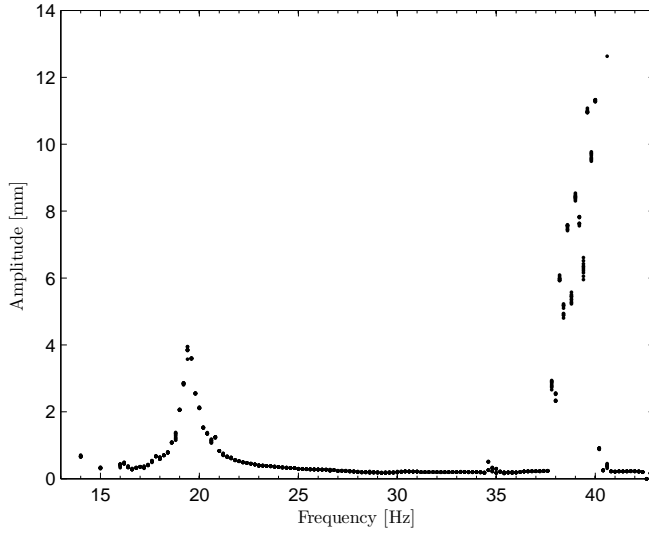
Fig. 8 Experimental frequency response diagram for the flat (y) direction, point P_y. Measured using stroboscopic sampling for a forcing amplitude of $F_o = 5.0$ N, frequency range Ω=[13, 43]

For both the flat and curved direction a 1/2 subharmonic resonance can be observed. This suggests that the nonlinearity generating the subharmonic behaviour is of the same kind in both cases. It is well documented in theory that quadratic type nonlinearities generate 1/2 subharmonic behaviours [2,3,19]. Therefore, for our equations of motion we choose this type of nonlinearity. Although other sub- and super-

Fig. 9 Experimentally recorded dynamic response for the flat (y) direction, point P_y of the plate. Force amplitude F_o=5 N, forcing frequency Ω=39.2 Hz. (a) displacement time response. (b) displacement power spectrum.

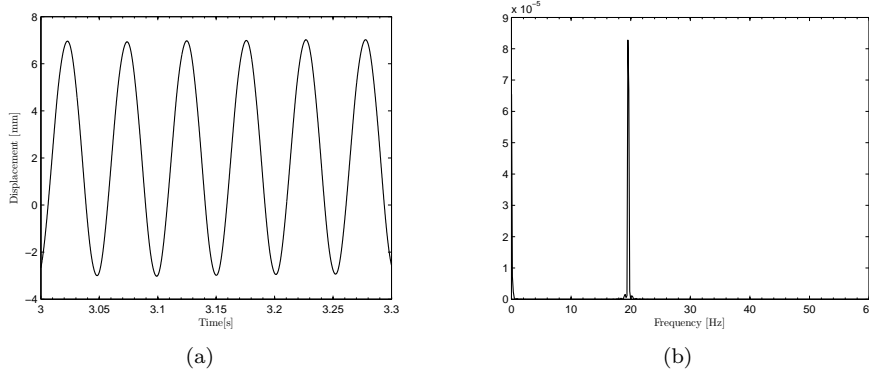harmonics were searched for both at lower and higher frequencies, no others could be found for the chosen levels of forcing and the current plate configuration. The equations of motion for each coordinate direction of the plate are discussed next.

2.3 Equations of Motion

For the curved direction of the plate two modes of vibration were observed in the frequency range of interest. Each mode was modelled with an ordinary differential equation. A quadratic nonlinearity for the restoring force and coupling between the modes was included to capture the observed subharmonic behaviour. The following is the system of equations of motion adopted

$$\ddot{x}_1 + 2\zeta_{x_1}\omega_{x_1}\dot{x}_1 + \omega_{x_1}^2 x_1 + \alpha_1 x_1^2 + \alpha_2 x_1 x_2 = \frac{f_{x_1}}{m}F_o \sin \Omega t, \qquad (1)$$

$$\ddot{x}_2 + 2\zeta_{x_2}\omega_{x_2}\dot{x}_2 + \omega_{x_2}^2 x_2 = \frac{f_{x_2}}{m}F_o \sin \Omega t, \qquad (2)$$

where x_1 is the out-of-plane displacement for mode X_1 with natural frequency ω_{x_1} = 17.6 Hz, x_2 is the out-of-plane displacement mode X_2 with natural frequency ω_{x_2} = 45.4 Hz, F_o is the driving force amplitude, Ω is the forcing frequency, f_{x_1} and f_{x_2} are the modal participation factor for modes X_1 and X_2 respectively, m is the mass of the plate, α_1 is the nonlinear quadratic restoring force coefficient, α_2 is the coupling coefficient between modes X_1 and X_2. The total out-of-plane displacement of point P_x is given by

$$x = \phi_{x_1}(x,y)_{P_x} x_1 + \phi_{x_2}(x,y)_{P_x} x_2 + \phi_{y_1}(x,y)_{P_x} y_1, \qquad (3)$$

where $\phi_{x_1}(x,y)_{P_x}$, $\phi_{x_2}(x,y)_{P_x}$ and $\phi_{y_1}(x,y)_{P_x}$ are the mode shapes associated with modes X_1, X_2 and Y_1 evaluated at point P_x.

Note that a single mode is sufficient to capture the dynamic behaviour of the flat direction. However, the subharmonic response is produced due to the coupling between

mode Y_1 and mode X_2, this nonlinear effect is included in our model as a quadratic coupling term. The modal equation identified for the flat direction (y) is

$$\ddot{y}_1 + 2\zeta_{y_1}\omega_{y_1}\dot{y}_1 + \omega_{y_1}^2 y_1 + \beta_1 {y_1}^2 + \beta_2 y_1 x_2 = \frac{f_{y_1}}{m}F_o\sin\Omega t, \tag{4}$$

where y_1 is the out-of-plane displacement mode Y_1 with natural frequency $\omega_{y_1} = 19.6$ Hz, F_o is the driving force amplitude, Ω is the forcing frequency, f_{y_1} is modal participation factor for mode Y_1, β_1 is the nonlinear quadratic restoring force coefficient, β_2 is the coupling coefficient between modes Y_1 and X_2. The total response in the flat direction is given by

$$y = \phi_{y_1}(x,y)_{P_y}y_1 + \phi_{x_1}(x,y)_{P_y}x_1 + \phi_{x_2}(x,y)_{P_y}x_2, \tag{5}$$

where $\phi_{x_1}(x,y)_{P_y}$, $\phi_{x_2}(x,y)_{P_y}$ and $\phi_{y_1}(x,y)_{P_y}$ are the mode shapes associated with modes X_1, X_2 and Y_1 evaluated at point P_y.

The coefficients proposed for the identified equations of motion were fitted using the frequency response diagrams obtained experimentally. First, the natural frequencies for each mode were chosen to coincide with the experimental data. Then, damping coefficients for each mode were calculated assuming a linear behaviour around the peak response for each of the identified modes. The nonlinear coefficients, α_i and β_i, were chosen to match the observed characteristics of the subharmonic resonance, such as triggering force amplitude and frequency width of the subharmonic resonance. The mode shape values, $\phi_{i_j}(x,y)_{P_n}$, were identified by inspecting the contribution to the total response of the plate by each mode in the frequency response diagrams at the measured points P_x and P_y. Finally, the coefficients f_{i_j} were fitted to have the closest displacement amplitude agreement with respect to the experimental responses measured. The identified coefficients are validated by obtaining simulation results for the dynamic response of the plate presented in the following section.

3 Simulation Results

The identified set of ordinary coupled nonlinear differential equations, equations (1), (2) and (4), were solved simultaneously using a Runge-Kutta type solver. Simulated frequency response diagrams are obtained using the stroboscopic sampling procedure applied to the displacement time series obtained from the numerical integration of the system equations. The simulated frequency response diagram obtained for point P_x for a forcing amplitude of 5 N is shown in figure 10. It shows the two modes of vibration at the measured frequencies, X_1 at 17.6 Hz and X_2 at 45.4 Hz. More importantly, the simulated results show the important subharmonic resonance. A very good agreement between the frequency range of the subharmonic response appearance is also achieved. In addition, the amplitude of the subharmonic oscillation coincides with the experimental results shown in section 2.2. The width of the peak of response obtained from the simulated frequency response diagrams for modes X_1 and X_2 show good agreement with the experimental results, validating the identified damping coefficients.

Figure 11 shows the simulated time series and power spectrum graphs calculated for point P_x. A non-harmonic response is observed that is very similar to the experimentally obtained one previously shown in figure 7. The power spectrum shows a response at the forcing frequency and at half the forcing frequency, which matches the experimental results for mode X_1.
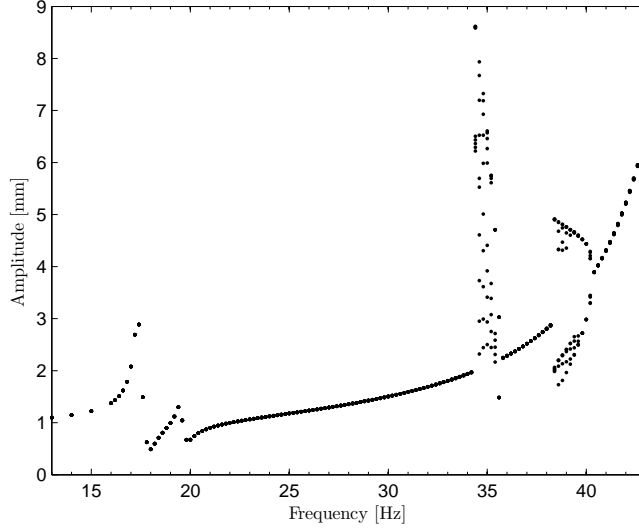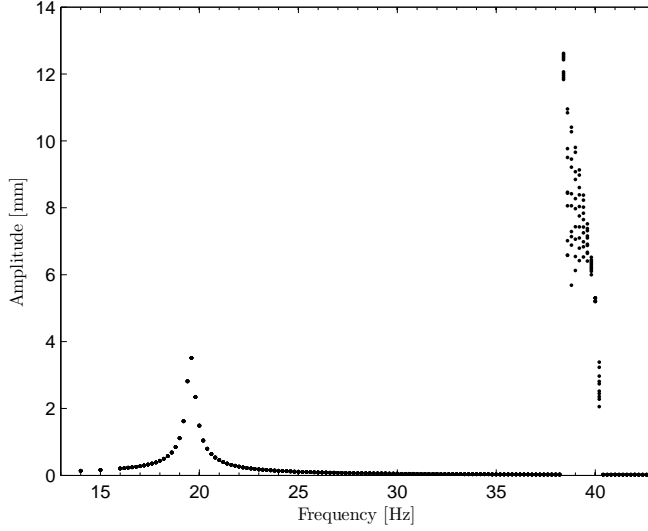
Fig. 10 Numerically simulated frequency response diagram for the curved (x) direction, equations (1) and (2). Simulation parameters: ω_{x_1}=17.45 Hz, ω_{x_2}=45.4 Hz, F_o=5.0 N, α_1=320000, α_2=640000, ζ_{x_1}=0.011, ζ_{x_2}=0.045, ζ_{y_1}=0.01, f_{x_1}=0.022, f_{x_2}=1.6, f_{y_1}=0.014, $\phi_{x_1}(x,y)_{P_x}$=0.4, $\phi_{x_2}(x,y)_{P_x}$=0.6, $\phi_{y_1}(x,y)_{P_y}$=0.4, m=0.135 kg, Ω=[13,43]

(a)   (b)
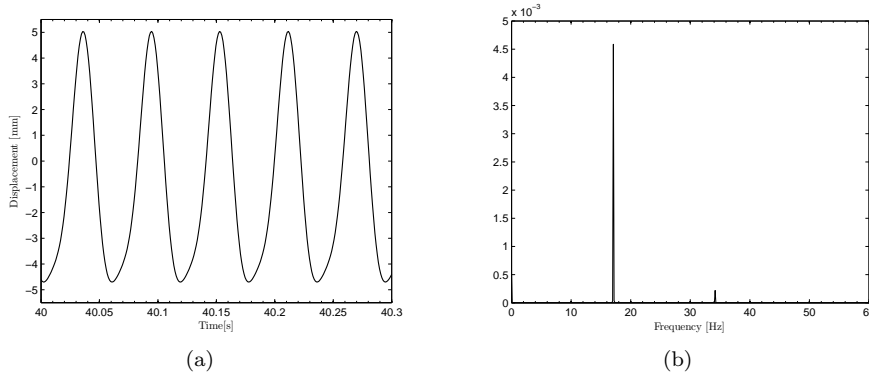
Fig. 11 Numerically simulated dynamic response for the curved (x) direction, equations 1 and 2. Forcing frequency $\Omega = 34.2$ Hz. Simulation parameters: ω_{x_1}=17.45 Hz, ω_{x_2}=45.4 Hz, F_o=5.0 N, α_1= 300000, α_2=640000, ζ_{x_1}=0.011, ζ_{x_2}=0.045, ζ_{y_1}=0.01, f_{x_1}=0.022, f_{x_2}=1.6, f_{y_1}=0.014, $\phi_{x_1}(x,y)_{P_x}$=0.4, $\phi_{x_2}(x,y)_{P_x}$=0.6, $\phi_{y_1}(x,y)_{P_y}$=0.4, m=0.135 kg. Sinusoidal wave response. a) displacement time response. b) displacement power spectrum.

The frequency response diagram for point P_y is shown in figure 12. As before, the simulation captures the observed key dynamic features of the experimental response, such as the natural frequencies and subharmonic response. The displacement time series and power spectrum graphs for the simulated subharmonic response range of mode Y_1, as shown in figure 13, are in very good agreement with those obtained experimentally.

Again a harmonic displacement time series is shown at half the forcing frequency as can be deduced by inspecting the power spectrum of the displacement, figure 13(b). The values of the modes shapes $\phi_{x_1}(x,y)_{P_y}$ and $\phi_{x_2}(x,y)_{P_y}$ are set to zero as there is no response from these modes present in the experimental frequency response diagram for the flat direction, see figure 8.

Fig. 12 Numerically simulated frequency response diagram for flat (y) direction, equation (4). Simulation parameters: ω_{y_1}=19.6 Hz, ω_{x_2}=45.4 Hz, F_o=5.0 N, β_1=650000, β_2=600000, ζ_{x_2}=0.045, ζ_{y_1}=0.01, f_{x_2}=1.6, f_{y_1}=0.014, $\phi_{y_1}(x,y)_{P_y}$=0.4, m = 0.135 kg, Ω=[11, 45].

4 Subharmonic Resonance Analysis

A theoretical study of the subharmonic resonance was conducted in order to further validate the form of the nonlinearities included in the proposed equations of motion presented in section 2.3. In addition this study allows for fine-tuning of the nonlinear and damping parameters, which are relatively difficult to fit accurately from experimental frequency response diagrams. The study consists of a comparison between the theoretically calculated and experimental boundary marking the onset of a subharmonic component within the response behaviour over the range of forcing amplitudes. We refer to this boundary as the instability boundary of the semi-trivial solution, where a semi-trivial solution contains a response at just the forcing frequency. Firstly equations of motion (1),(2) and (4) are scaled and detuning is introduced such that the response in the region around twice the natural frequencies of modes X_1 and Y_1 can be studied. A first order averaging process is performed to derive first-order differential-equations for the response. These equations are then analysed to study the local stability of the selected modes in the presence of external harmonic excitation [11]. The resulting
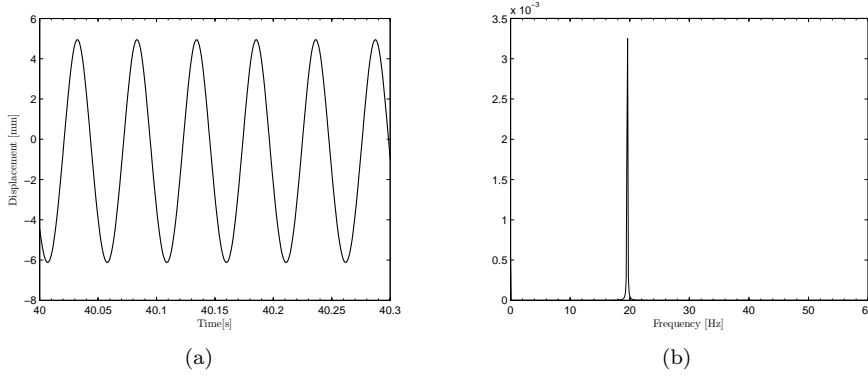
Fig. 13 Numerically simulated dynamic response for flat (y) direction. Forcing frequency Ω = 39.2 Hz. Simulation parameters: ω_{y_1}=19.6, ω_{x_2}=45.4, F_o=5.0 N, β_1=650000, β_2=600000, ζ_{x_2}=0.045, ζ_{y_1}=0.01, f_{x_2}=1.6, f_{y_1}=0.014, $\phi_{y_1}(x,y)_{P_y}$=0.4, m=0.135 kg. a) displacement time response. b) displacement power spectrum.

stability boundaries obtained are plotted in parameter space to show the regions of stability and instability for each of the modes under consideration.

4.1 Scaling and Averaging

The equations of motion of the system are scaled so that the dynamics are dominated by the undamped linear response. This is achieved by introducing the small parameter ϵ and arranging the equations to take the following standard Lagrange form

$$\ddot{z}(t) + \omega^2 z(t) = \epsilon F(z(t), \dot{z}(t), t). \tag{6}$$

To study the subharmonic response for mode X_1 the forcing frequency must be close to twice the natural frequency, ω_{x_1}. This requires the forcing frequency to be $\Omega = 2\omega_{x_1}(1 + \epsilon\mu)$, where μ is the frequency detuning and ϵ is a small parameter. Finally, we introduce the time transform

$$\tau = (1 + \epsilon\mu)t \tag{7}$$

to equation (1) to obtain the scaled and th transformed equations of motion

$$x_1'' + \omega_{x_1}^2 x_1 + \epsilon[2\zeta_{x_1}\omega_{x_1}x_1' + 2\mu\omega_{x_1}^2 x_1 + \alpha_1 x_1^2 + \alpha_2 x_1 x_2 - \frac{f_{x_1}}{m}Fo\sin 2\omega\tau] = \mathcal{O}(\epsilon^2), \tag{8}$$

where $\{\}'$ represents the derivative with respect to scaled time τ.

Using the transformation [28]

$$x(t) = x_a \cos(\omega t) + x_b \sin(\omega t), \tag{9}$$

$$\dot{x}(t) = x_a\omega \sin(\omega t) + x_b\omega \cos(\omega t), \tag{10}$$

and the Lagrange standard form, equation (6), gives

$$\dot{x}_a = -\frac{\epsilon}{\omega}F(\dot{x}(t), x(t), t)\sin(\omega t),$$
$$\dot{x}_b = \frac{\epsilon}{\omega}F(\dot{x}(t), x(t), t)\cos(\omega t). \tag{11}$$

We can obtain approximate solutions for equation (8) by a standard averaging procudure [27]. As mode X_1 is lightly damped its response away from its natural frequency is very close to zero. Therefore, zero response is assumed for the approximate solutions in the studied range for the forcing frequency, that is for $\Omega \approx 2\omega_{x_1}$. Using the standard form (11) for the scaled equation (8) and applying averaging over the scaled time period $\frac{2\pi}{\omega_{x_1}}$ in τ (which corresponds to a time period of two cycles of frequency Ω in real-time t) we find the of averaged equations for mode X_1

$$x1'_{a_{avg}} = -\frac{\epsilon}{\omega_{x_1}}[\zeta_{x_1}\omega_{x_1}^2 x1_{a_{avg}} - \frac{\alpha_2}{4}x1_{a_{avg}}x2_{b_{avg}} + \frac{\alpha_2}{4}x1_{b_{avg}}x2_{a_{avg}} - \mu\omega_{x_1}^2 x1_{b_{avg}}],$$
$$x1'_{b_{avg}} = \frac{\epsilon}{\omega_{x_1}}[-\zeta_{x_1}\omega_{x_1}^2 x1_{b_{avg}} - \frac{\alpha_2}{4}x1_{b_{avg}}x2_{b_{avg}} - \frac{\alpha_2}{4}x1_{a_{avg}}x2_{a_{avg}} - \mu\omega_{x_1}^2 x1_{a_{avg}}], \tag{12}$$

where the subscript a and b refer to cosine and sine component of the Lagrange form (11) respectively and again $\{\}'$ represents the derivative with respect to scaled time τ. The subscript avg indicates that the terms have been averaged over a cycle of ω_{x_1} in the scaled τ for mode X_1.

Similar averaged equations can be obtained for the Y_1 mode, where the frequency detuning $\Omega = 2w_{y_1}(1 + \epsilon\nu)$ is applied, with the corresponding time transform

$$T = (1 + \epsilon\nu)t, \tag{13}$$

giving

$$y1_{a_{avg}}^* = -\frac{\epsilon}{\omega_{y_1}}[\zeta_{y_1}\omega_{y_1}^2 y1_{a_{avg}} - \frac{\beta_2}{4}y1_{a_{avg}}y2_{b_{avg}} + \frac{\beta_2}{4}y1_{b_{avg}}y2_{a_{avg}} - \nu\omega_{y_1}^2 y1_{b_{avg}}],$$
$$y1_{b_{avg}}^* = \frac{\epsilon}{\omega_{y_1}}[-\zeta_{y_1}\omega_{y_1}^2 y1_{b_{avg}} - \frac{\beta_2}{4}y1_{b_{avg}}y2_{b_{avg}} - \frac{\beta_2}{4}y1_{a_{avg}}y2_{a_{avg}} - \nu\omega_{y_1}^2 y1_{a_{avg}}], \tag{14}$$

where $\{\}^*$ represents the derivative with respect to scaled time T. Note that the averaging is now applied over the scaled time period $\frac{2\pi}{\omega_{y_1}}$ in T, equivalent to two cycles of Ω in real-time t.

4.2 Stability analysis

The boundary of the semi-trivial solution, this is $x1_{avg}$=0 and $y1_{avg}$=0 where there is no subharmonic response, in parameter space is obtained by studying the localized stability of each of the modes. For mode X_1 we can write the averaged system (12) in matrix form as

$$\begin{pmatrix} x1'_{a_{avg}} \\ x1'_{b_{avg}} \end{pmatrix} = \epsilon \begin{bmatrix} \frac{\alpha_2}{4\omega_{x_1}}x2_{b_{avg}} - \zeta_{x_1}\omega_{x_1} & \mu\omega_{x_1} - \frac{\alpha_2}{4\omega_{x_1}}x2_{a_{avg}} \\ -\mu\omega_{x_1} - \frac{\alpha_2}{4\omega_{x_1}}x2_{a_{avg}} & -\frac{\alpha_2}{4\omega_{x_1}}x2_{b_{avg}} - \zeta_{x_1}\omega_{x_1} \end{bmatrix} \begin{pmatrix} x1_{a_{avg}} \\ x1_{b_{avg}} \end{pmatrix}. \tag{15}$$

From system (15) the localized stability about $x_{1_{avg}}=0$ can be found by studying the matrix eigenvalues, which are given by

$$\lambda^2 + 2\zeta_{x_1}\omega_{x_1}\lambda + (\zeta_{x_1}\omega_{x_1})^2 + (\mu\omega_{x_1})^2 - \frac{(\alpha_2 x_{2_{avg}})^2}{(4\omega_{x_1})^2} = 0, \tag{16}$$

where $x_{2_{avg}}^2 = x_{2_{a_{avg}}}^2 + x_{2_{b_{avg}}}^2$. Given that $\zeta_{x_1}\omega_{x_1}^2 > 0$, the boundary of local instability of the zero amplitude response occurs when $\lambda = 0$. This corresponds to the region in which a non-zero response at frequency ω_{x_1}, the subharmonic frequency, will occur. For $\lambda = 0$ the characteristic equation (16) simplifies to

$$x_{2_{avg}} \geq \frac{4\omega_{x_1}^2}{\alpha_2}\sqrt{\zeta_{x_1}^2 + \mu^2}. \tag{17}$$

By solving the linear mode X_2, equation (2), at the forcing frequency $\Omega = 2\omega_{x_1}(1+\epsilon\mu)$ we find the force that triggers the appearance of the subharmonic response for mode X_1

$$F_o \geq \frac{4\omega_{x_1}^2}{\alpha_2}\frac{f_{x_2}}{m}\sqrt{\zeta_{x_1}^2 + \mu^2}\sqrt{(\omega_{x_2}^2 - \Omega^2)^2 + (2\zeta_{x_2}\omega_{x_2}\Omega)^2}. \tag{18}$$

Applying the same stability analysis approach to mode Y_1 averaged equations (14), we find a subharmonic to be present for

$$x_{2_{avg}} \geq \frac{4\omega_{y_1}^2}{\beta2}\sqrt{\zeta_{y_1}^2 + \nu^2}. \tag{19}$$

Also as with mode X_1, the linear X_2 modal response at which a subharmonic of mode Y_1 appears can be related to the forcing as

$$F_o \geq \frac{4\omega_{y_1}^2}{\beta_2}\frac{f_{x_2}}{m}\sqrt{\zeta_{y_1}^2 + \nu^2}\sqrt{(\omega_{x_2}^2 - \Omega^2)^2 + (2\zeta_{x_2}\omega_{x_2}\Omega)^2}. \tag{20}$$

4.3 Subharmonic Stability Boundaries

Equations 18 and 20 give the theoretical force amplitude required to trigger subharmonic oscillations of the X_1 and Y_1 modes respectively. The experimental subharmonic response range for a given forcing amplitude can be directly measured from experimental frequency response diagrams for various levels of forcing. The lower and higher frequency limits for the subharmonic response are obtained and plotted for each experimental forcing amplitude for both modes X_1 and Y_1. These results are plotted as crosses and circles for modes X_1 and Y_1 respectively in figure 14. For the case of the theoretical boundaries, after minor fine-tuning of the damping and nonlinear parameters identified using the frequency response plots, there is good agreement with the experimental results. These theoretical boundaries are shown in figure 14 as solid and dashed lines for modes X_1 and Y_1 respectively. In the case of the higher frequency limits of the boundaries it can be seen that at higher forcing amplitudes there is a deterioration in the agreement between the theoretical and experimental behaviour. One possible explanation for this is that the system exhibits hysteretic behaviour, as has been observed in other experimental studies of nonlinear systems such as that reported in [11]. To investigate this the experiments were repeated, however this time for
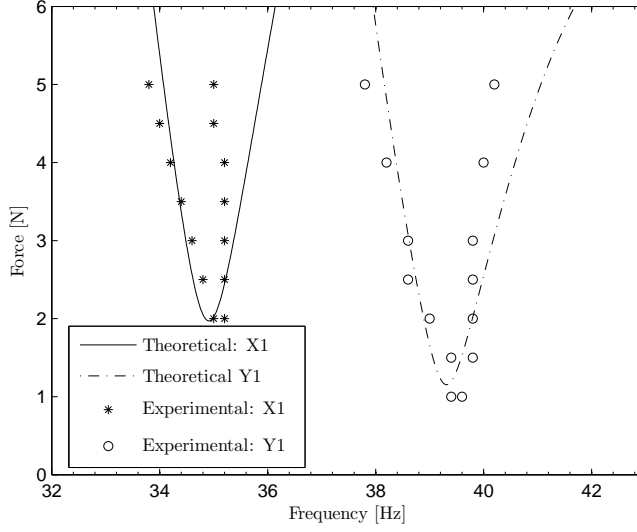
Fig. 14 Stability Boundaries: comparison between the theoretical prediction and the experimentally measured range for the subharmonic resonance of modes X_1 and Y_1. Parameters used to solve equations (18) and (20): ω_{x_1}=17.45, ω_{x_2}= 45, ω_{y_1}=19.6, α_2=680000, β_2=680000, ζ_{x_1}=0.011, ζ_{x_2}=0.047, ζ_{y_1}=0.008, f_{x_2}=1.7, m=0.135 kg

each level of forcing the frequency was stepped down incrementally from a frequency higher than the stability boundary (rather than stepped up from a frequency below the boundary). In addition tests were performed in which the frequency was kept constant and the forcing was stepped up incrementally. The experimental results showed that the boundary of instability was the same regardless of the direction in which it was approached in the amplitude-frequency space This result indicates that the system does not exhibit hysteresis around these boundaries.

Figures 15(a) and 15(b) show the simulated frequency response diagrams obtained using the fine-tuned parameters used for the theoretical boundaries, which still show good agreement with the experimental results, shown in figures 6 and 8. This indicates that the slight parameter changes used to obtain the fine-tuned fit in figure 14 are consistent with the original experimental data, proving the robustness of the identified model.

5 Conclusions

A simple low order model to capture the key dynamic features for a bi-stable composite plate was successfully identified based on a system identification approach. The plate response was captured using a modal approach which rendered simple nonlinear differential equations for each of the identified modes. An excellent qualitative match between the experimental and the simulated frequency response diagrams was obtained. The very important subharmonic behaviour was captured with the nonlinearities included in the presented model as well as the natural frequencies for the modes on the studied range of frequency. Moreover, a good quantitative match for the amplitude of
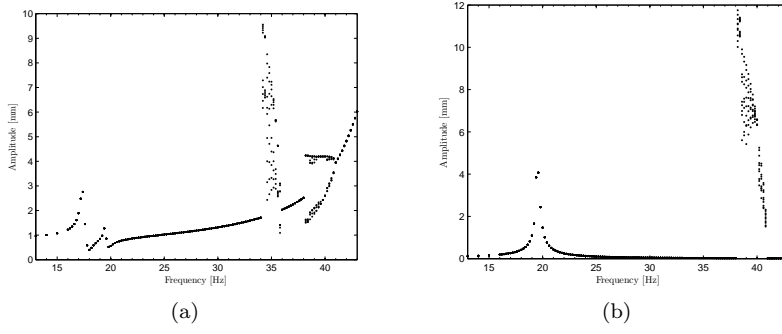
Fig. 15 a) Numerically simulated frequency response diagram for the curved (x) direction, equations (1) and (2). Simulation parameters: ω_{x_1}=17.45 Hz, ω_{x_2}=45 Hz, F_o=5.0 N, α_1=300000, α_2=680000, ζ_{x_1}=0.011, ζ_{x_2}=0.047, ζ_{y_1}=0.008, f_{x_1}=0.022, f_{x_2}=1.7, f_{y_1}=0.014,$\phi_{x_1}(x,y)_{P_x}$=0.4, $\phi_{x_2}(x,y)_{P_x}$=0.6, $\phi_{y_1}(x,y)_{P_y}$=0.4, m=0.135 kg, Ω=[13,43]. b) Numerically simulated frequency response diagram for flat (y) direction, equation (4). Simulation parameters: ω_{y_1}=19.6, ω_{x_2}=45, F_o=5.0 N, β_1=680000, β_2=680000, ζ_{x_2}=0.047, ζ_{y_1}=0.008, f_{x_1}=0.022, f_{x_2}=1.7, f_{y_1}=0.014, $\phi_{y_1}(x,y)_{P_y}$=0.4, m=0.135 kg, Ω=[13,43].

the response of both the linear and nonlinear response was achieve by including one mode to describe the flat (y) direction dynamics, and two for the curved (x) direction of the plate. Time series and power spectrum graphs for the experimental and simulated results confirm the close match achieved seen in the frequency response diagrams.

Using the derived equations and applying averaging techniques the stability of the subharmonic resonance for modes X_1 and Y_1 was studied obtaining very good agreement. For both modes the force required to trigger the subharmonic oscillation as well as the lower frequency boundaries were closely matched. The theoretical results for the higher frequency boundary of the instability differ slightly from the experimental data as the forcing amplitude increases, however this frequency mismatch is regarded as small when compared to the capability of the model to capture the complex dynamics of the bi-stable plate for a much larger range of frequencies and forcing amplitudes.

The identification method used to derive the equations of motion can be extended to similar systems where the response can be measured and the nonlinear behaviour compared to the established theory. The ability to capture complex dynamic behaviour exhibited by bi-stable composites with simple mathematical models will enable us to enhance their applicability in the design of morphing structures. In addition, low order control strategies for vibration suppression and actuation can be more easily implemented due to the simplicity of the dynamic models to be developed for such structures. New developments will seek to couple the snap-through and the stable-state dynamics studied in this paper to formulate a complete model for the global response of the bi-stable plate.

References

1. Arrieta, A.F., Mattioni, F., Neild, S.A., Weaver, P.M., Wagg, D.J., and Potter K.: Nonlinear dynamics of a bi-stable composite laminate plate with applications to adaptive structures. In: 2nd European Conference for Aero-Space Sciences(EUCASS2007), Brussels, July (2007)
2. Balachandran, B. and Nayfeh, A.H.: Observations of Modal Interactions in Resonantly Forced Beam-Mass Structures. Nonlinear Dyn. 2, 77-117 (1991)
3. Chen, S.H., Cheung, Y.K. and Xing, H.X.: Nonlinear Vibration of Plane Structures by Finite Element and Incremental Harmonic Balance Method. Nonlinear Dyn. 26, 87-104 (2001)
4. Clark, R.L., Saunders, W.R. and Gibbs, G.P.: Adaptive structures: Dynamics & Control. Wiley, New York (1998)
5. Dano, M.-L. and Hyer, M.W.: Thermally-induced deformation behavior of unsymmetric laminates. Int. J. Solids Struct. 35, 2101-2120 (1998)
6. Dano, M.-L. and Hyer, M.W.: Snap-through of unsymmetric fiber-reinforced composite laminates. Int. J. Solids Struct. 39, 175-198 (2002)
7. Dano, M.-L. and Hyer, M.W.: SMA-induced snap-through of unsymmetric fiber-reinforced composite laminates. Int. J. Solids Struct. 40, 5949-5972 (2003)
8. Emam, S.A. and Nayfeh, A.H.: Nonlinear Responses of Buckled Beams to Subharmonic-Resonance Excitations. Nonlinear Dyn. 35, 105-122 (2004)
9. Ewins. D.J.: Modal Testing. Res. Stud. Press LTD, Baldock (2000)
10. Giddings, P., Bowen, C.R., Butler, R. and Kim, H.A.: Characterisation of actuation properties of piezoelectric bi-stable carbon-fibre laminates . Composites. Part. A. 39, 697-703 (2008)
11. Gonzalez-Buelga, A., Neild, S.A., Wagg, D.J. and Macdonald, J.H.G.: Modal stability of inclined cables subjected to vertical support excitation. J. Sound Vib. 318, 565-579 (2008)
12. Hufenbach, W., Gude, M., Kroll, L.: Design of multistable composites for application in adaptive structures. Composites Science and Technology. Compos. Sci. Technol. 62, 22012207 (2002)
13. Kerschena, G., Worden, K., Vakakis, A. F. and Golinval, J.-C.: Past, present and future of nonlinear system identification in structural dynamics. Mech. Syst Signal. Pr. 20, 505592 (2006)
14. Lefschetz, S.: Modern Mathematics for the Engineer. Mcgraw-Hill, New York (1956)
15. Liu, J., D. T. Martin, D. T., K. Kadirvel, T. Nishida, Cattafesta, L., Sheplak M., and Mann, B. P.: Nonlinear model and system identification of a capacitive dual-backplate MEMS microphone. J. Sound Vib. 309, 276-292 (2008)
16. Mattioni, F., Weaver, P.M., Potter K. and Friswell, M.I.: The application of residual stress tailoring of snap-through composites for variable sweep wings. In: 47th AIAA/ASME/ASCE/AHS/ASC Structures, Structural Dynamics, and Materials Conference, Rhode Island, May (2006)
17. Mattioni, F., Weaver, P.M., Potter K. and Friswell, M.I.: Analysis of thermally induced multistable composites. Int. J. Solids Struct. 45, 657675 (2008)
18. Nayfeh, A.H.: Nonlinear Interactions, Analytical, Computational, and Experimental Methods. Wiley, New York (2000)
19. Nayfeh, A.H.: Introduction to Perturbation Techniques. Wiley, New York (1981)
20. Nayfeh, A.H. and Mook, D.T.: Nonlinear Oscillations. Wiley, New York (1979)
21. Oh, I.K., Han, J.H. and Lee, I.: Thermopiezoelastic Snapping of Piezolaminated Plates Using Layerwise Nonlinear Finite Elements. AIAA Journal. 39, 1188-1197 (2001)
22. Potter, K., Weaver, P. , Seman, A.A., and Shah, S.: Phenomena in the bifurcation of unsymmetric composite plates. Composites Part A. 35, 100-106 (2006)
23. Potter, K.K and Weaver, P.M.: A concept for the generation of out-of-plane distortion from tailored FRP laminates. Composites Composites Part A. 35, 1353-1361 (2004)
24. Schultz, M.R. and Hyer, M.W., Snap-through of Unsymmetric Cross-ply Laminates using Piezoceramic Actuators. J. Intell. Mater. Syst. Struct. 14, 795-814 (2003)
25. Schultz, M.R., Hyer, M.W., Williams, R.B., Wilkie, W.K. and Inman, D.J.: Snap-through of unsymmetric laminates using piezocomposite actuators. Composite Sci. Tech. 66, 2442-2448 (2006)
26. Sokorin, S.V. and Terentiev, A.V.: On Modal Interaction, Stability and Nonlinear Dynamics of a Model Two D.O.F. Mechanical System Performing Snap-Through Motion. Nonlinear Dyn. 16, 239-257 (1998)
27. Tondl, A., Ruijgrok, T., Verhuslt, F. and Nabergoj, R.: Autoparametric Resonance in Mechanical Systems. Camb. Univ. Press, Cambridge (2000)

28. Verhulst, F.: Nonlinear Differential Equations and Dynamical Systems. Springer, (1996)
29. Von Karman, T.: The Engineer Grapples With Nonlinear Problems. Bull. Amer. Math. Soc. 46, 615-683 (1940)